

Article

Chitosan-Functionalized $Mg_{0.5}Co_{0.5}Fe_2O_4$ Magnetic Nanoparticles Enhance Delivery of 5-Fluorouracil In Vitro

Sanele Mngadi ¹, Seipati Mokhosi ^{1,*}, Moganavelli Singh ¹  and Wendy Mdlalose ²

¹ Discipline of Biochemistry, University of Kwazulu-Natal, Private Bag X54001, South Africa; 218086937@stu.ukzn.ac.za (S.M.); singhm1@ukzn.ac.za (M.S.)

² Discipline of Physics, University of Kwazulu-Natal, Private Bag X54001, South Africa; MdlaloseW@ukzn.ac.za

* Correspondence: mokhosis@ukzn.ac.za

Received: 2 April 2020; Accepted: 27 April 2020; Published: 2 May 2020



Abstract: Magnetic nanoparticles (MNPs) have been widely investigated as a strategy to improve the delivery efficiency of therapeutic and diagnostic agents. Substituted iron oxides or ferrite nanoparticles (NPs) such as $CoFe_2O_4$ represent an interesting and novel class of MNPs, although they are under-researched in the field of biomedicine. In this study, chitosan-functionalized $Mg_{0.5}Co_{0.5}Fe_2O_4$ NPs were loaded with the anti-cancer 5-fluorouracil (5-FU) drug to yield CS- $Mg_{0.5}Co_{0.5}Fe_2O_4$ -5FU. Transmission electron microscopy (TEM), Fourier Transform infra-red (FTIR) spectroscopy and nanoparticle tracking analysis (NTA) were employed to determine the physiochemical properties of the NPs. Physico-chemical characterizations confirmed spherical NPs with particle sizes of approximately 20.39 nm. Improved colloidal stability was observed, as determined by a zeta potential of approximately -20 mV for the drug-loaded CS- $Mg_{0.5}Co_{0.5}Fe_2O_4$ NPs. Drug encapsulation efficiencies of $>60\%$ were attained, showing a pH-dependent release of 5-FU. Cell viabilities investigated using the 3-[(4,5-dimethylthiazol-2-yl)-2,5-diphenyl tetrazolium bromide] (MTT) and sulforodhamine B (SRB) assays in human embryonic kidney (HEK293), human breast adenocarcinoma (MCF-7) and human cervical cancer (HeLa) cells showed that these drug-loaded NPs exhibited more targeted tumor-specific cytotoxicities compared to free drugs. CS- $Mg_{0.5}Co_{0.5}Fe_2O_4$ -5FU NPs displayed significant targeted delivery potential to the investigated cancer cell lines. Conclusively, these results suggest that the CS- $Mg_{0.5}Co_{0.5}Fe_2O_4$ -5FU NPs are promising therapeutic delivery systems in anti-cancer treatment.

Keywords: magnetic nanoparticles; chitosan; cytotoxicity; drug loading; anti-cancer

1. Introduction

The efficient delivery of anti-cancer therapeutics with minimal toxicity in healthy organs or tissues remains an enormous challenge [1]. Current conventional therapies often result in off-target delivery, leading to undesired side-effects [2]. Magnetic iron oxides that have been extensively studied in the field of biomedicine and cancer therapy include maghemites ($\gamma-Fe_2O_3$) and magnetites (Fe_3O_4), due to their biocompatibility [3].

Spinel ferrites (MFe_2O_4) are an emerging and exciting class of iron oxide nanoparticles (NPs), due to their attractive and unique properties such as chemical stability and high saturation magnetization [4]. However, limitations relating to colloidal stability, toxicity (such as in cobalt-based NPs) and solubility render them unpopular [4]. The optimization of key parameters such as size, charge and surface chemistry is often employed to tailor the NPs for desired applicability. Additionally, substituting other metallic ions into a $CoFe_2O_4$ NP lattice may also favorably alter their various structural and magnetic properties [5,6]. In cancer diagnosis and chemotherapy, the use of these NPs has resulted in site-specific

delivery of anti-tumor agents adsorbed on the surface of MNPs without compromising healthy tissue in the body [7].

One of the main challenges in the application of magnetic NPs relates to their inherent propensity to aggregate, resulting in short-term stability when in biological suspensions. This is mainly the result of clearance by the macrophage system and subsequent reduced circulation time [7,8]. These challenges are often resolved by modifications to the NPs by functionalization with suitable polymers such as chitosan, dextran, polyethylene glycol and others [9].

Chitosan is one of the most abundant naturally occurring polymers, and is derived as a deacetylated form of chitin. The amino and hydroxyl groups present on its surface confer its cationic nature. These also allow for the NPs to be further functionalized [10,11]. Owing to the low immunogenicity and biodegradability of chitosan, it has attracted a great deal of attention as a functional biopolymer in the pharmaceutical and biomedical applications and industry [12,13]. Coupling chitosan to NPs has been observed to result in controlled drug release [12], muco-adhesion [14], in situ gelation [15], antimicrobial activity [16] and permeation enhancement [17,18].

Recently, the use of chitosan-functionalized MNPs as a delivery system for the sustained release of 5-fluorouracil (5-FU) was reported to resolve the short half-life of chemotherapeutic drugs [19]. 5-FU singularly, or in combination with chemotherapy agents, exhibits a broad spectrum of activity against solid tumors of the gastrointestinal tract, pancreas, ovary, liver, brain, breast etc. The mechanism behind the cytotoxicity and cell death caused by 5-FU is its interference with nucleoside metabolism in RNA and DNA [20].

In the present investigation, $Mg_{0.5}Co_{0.5}Fe_2O_4$ NPs were coated with chitosan and characterized using various analytical techniques. Furthermore, they were investigated for the drug release potential of 5-FU, and cytotoxicities assays were performed in human embryonic kidney (HEK293), human breast adenocarcinoma (MCF-7) and human cervical cancer (HeLa) cells.

2. Experimental Details

2.1. Materials

Cobalt chloride tetrahydrate ($CoCl_2 \cdot 4H_2O$, 98%), iron (III) chloride tetrahydrate ($FeCl_2 \cdot 4H_2O$, 98%), magnesium chloride hexahydrate ($Cl_2Mg \cdot 6H_2O$, 99%), 5 M NaOH, $AgNO_3$, ethylene glycol ($(CH_2OH)_2$, 99%), Chitosan from shrimp shells (MWCO 50,000–190,000 Da) ($C_6H_{11}NO_4$) $_n$, $\geq 75\%$ deacetylation and 5-Fluorouracil (5-FU), as well as dialysis tubing (MWCO 12,000 Daltons), were purchased from Sigma-Aldrich, St. Louis, MO, USA. 3-[(4,5-dimethylthiazol-2-yl)-2,5-diphenyl tetrazolium bromide] (MTT), sulforodhamine B (SRB Dye, $C_{27}H_{30}N_2O_7S_2$, Mw: 558.67 g mol⁻¹), phosphate-buffered saline tablets (PBS [140 mM NaCl, 10 mM phosphate buffer, 3 mM KCl]), acridine orange (AO) hemi (zinc chloride) salt [3,6-Bis(dimethylamino) acridine hydrochloride zinc chloride double salt] ($C_{17}H_{19}N_3$, Mw: 265.36, g mol⁻¹), ethidium bromide, glacial acetic acid and dimethyl sulfoxide (DMSO) were sourced from Merck (Darmstadt, Germany). Eagle's Minimum Essential Medium (EMEM), L-glutamine (4.5 g L⁻¹), trypsin-versene and antibiotics (penicillin [10,000 U/mL], streptomycin [10,000 µg/mL], amphotericin B [25 µg/mL]) were acquired from Lonza Bio-Whittaker (Walkersville, MD, USA). Fetal bovine serum (FBS) was used (Hyclone, UT, USA). Human embryonic kidney cells (HEK293) was sourced from the University of the Witwatersrand (Anti-viral Gene Therapy Unit, Johannesburg, South Africa). Human breast adenocarcinoma (MCF-7) and human cervical cancer (HeLa) were obtained from American Type Culture Collection (ATCC) (Manassas, VA, USA). All sterile tissue culture plasticware were obtained from Corning Inc. (New York, NY, USA). All biological assays were conducted under aseptic conditions in an Airvolution Class II biosafety laminar flow hood. Chemical reagents of analytical quality were used in this study without any further purification, and ultrapure 18 MΩ Milli-Q water (pH 6.8) was used throughout.

2.2. MNPs Synthesis

Pure $\text{Mg}_{0.5}\text{Co}_{0.5}\text{Fe}_2\text{O}_4$ NPs were synthesized using the glycol-thermal method, as previously reported [21]. Calculated stoichiometric measurements of 2.0818 g of $\text{CoCl}_2 \cdot 4\text{H}_2\text{O}$, 9.4854 g of $\text{FeCl}_2 \cdot 4\text{H}_2\text{O}$ and 1.0971 g of $\text{Cl}_2\text{Mg} \cdot 6\text{H}_2\text{O}$ were weighed out and dissolved in 500 mL of deionized water. The homogenous solution was placed on a magnetic stirrer and the initial pH was recorded. The solution was stirred continuously for a duration of 30 min. Precipitation of the metal chlorides was carried out by the gradual addition of 5 M NaOH solution until a pH of 9 was reached. The precipitate was finally washed thoroughly to remove the unwanted chlorides. The wash steps were carried out using a Whatman (GF/F 110 mm) glass microfiber filter in a Büchner funnel. AgNO_3 was added to the washed solute to detect the presence of chlorides. A clear and non-cloudy solute indicated that all chlorides were removed. Thereafter, the washed precipitate was collected and submerged into 250 mL of ethylene glycol solution, and then placed in a PARR 4843 stirred pressure reactor and allowed to run for 6 h at a soak temperature of 200 °C with a stirring speed of 300 rpm and 80 psi pressure. The final product obtained was rinsed with 200 mL of ethanol over Whatman paper, and finally placed under a 200 W infrared light and allowed to dry overnight. The dried samples were then homogenized using an agate mortar and pestle.

2.3. Coating of Magnetic Nanoparticles

The synthesized $\text{Mg}_{0.5}\text{Co}_{0.5}\text{Fe}_2\text{O}_4$ MNPs were coated with chitosan (CS), as reported previously [21]. Briefly, 0.5 g of chitosan was weighed out and dissolved in 100 mL of acetic acid for a 0.5% chitosan solution. Approximately 10 M NaOH solution was then added dropwise to the prepared solution, until a pH of 4.8 was attained. Thereafter, 0.2 g of the synthesized MNPs was dissolved in the chitosan solution, and the resulting mixture sonicated using a Scientech Ultrasonic bath (Randburg, South Africa) at 60 °C for an hour. The mixture was then transferred into a beaker and stirred mechanically using an IKA RW 20 Digital Dual-Range Mixer System (Staufen, Germany) for 18 h at room temperature. The black homogeneous mixture attained was separated by centrifugation at 3000 rpm for 30 min. The sample was centrifuged five times, with a deionized water wash between each centrifugation. The chitosan-coated MNPs ($\text{CS-Mg}_{0.5}\text{Co}_{0.5}\text{Fe}_2\text{O}_4$) were then dispersed in a petri dish, left to dry at room temperature, and finally homogenized using an agate mortar and pestle.

2.4. Characterization of Synthesized MNPs

Transmission electron microscopy (TEM) measurements were carried out using a JEOL JEM-1010 TEM (Tokyo, Japan) operated at an accelerated voltage of 100 kV. The MegaView III Soft Imaging Systems (SIS) (JEOL JEM 1010, Tokyo, Japan) side-mounted 3-megapixel digital camera was used to document the micrographs. Surface morphology of the nanoparticles was investigated using scanning electron microscopy (SEM). Samples were coated with gold using a Q150R Rotary-Pumped Sputter Coater (Leica Microsystems, Wetzlar, Germany) and viewed under a Zeiss Ultra Plus FE-SEM (ZEISS Field Emission Scanning Electron Microscope, Oberkochen, Germany) at a magnification of 3500 \times .

A Perkin Elmer Spectrum 100 FTIR (Fourier Transform Infrared) spectrometer (Waltham, MA, USA) was used for the FTIR analyses in which a Universal Attenuated Total Reflectance (ATR) component was bound to it. The analyses were performed in the range of 380–4000 cm^{-1} at a resolution of 4 cm^{-1} in room temperature at four scans per measurement. The data were generated using Spectrum[®] 10 Software. Small amounts of the uncoated and coated MNPs were loaded onto the ATR crystal. To guarantee interaction amongst the nanoparticle samples and the crystal, a pressure of 120 psi was exerted. Zeta potential and hydrodynamic size distributions of the nanoparticles was carried by nanoparticle tracking analysis (NTA) using a NanoSight NS500 (Malvern Instruments, Worcestershire, UK) at 25 °C. Analyses were performed using the NanoSight NTA version 3.2 software.

2.5. Drug Encapsulation Efficiency (EE)

Drug loading of the nanoparticles was adapted from that which was previously reported [10]. Briefly, the synthesized MNPs CS-Mg_{0.5}Co_{0.5}Fe₂O₄ was loaded with 5-FU by dissolving 10 mg of the dried nanoparticle in 25 mL of a drug solution (0.2 mg/mL in PBS, pH 7.4). This was then placed on an orbital shaker at 200 rpm for 48 h at room temperature. To assess the drug encapsulation efficiency (EE), the drug-loaded nanocomposites CS-Mg_{0.5}Co_{0.5}Fe₂O₄-5-FU were separated from the solution using an external magnetic field, and oven-dried at 40 °C overnight. The concentration of 5-FU in the obtained supernatants was determined from a calibration curve by measuring the UV absorbance at 266 nm. The EE was estimated using the following equation:

$$EE (\%) = \frac{5\text{-FU}_{\text{total}} - 5\text{-FU}_{\text{supernatant}}}{5\text{-FU}_{\text{total}}} \times 100$$

2.6. Drug Release Studies

To determine the drug release profile, 3 mg of the drug-loaded nanocomposites in 10 mL PBS were dispensed into dialysis tubings (12,000 MWCO), and suspended in separate beakers containing 20 mL of PBS at pH 4.5, 6.5 and 7.4, respectively. The temperature was maintained under shaking conditions at 37 °C. At specific time intervals, 2 mL of the dialysates were withdrawn to determine the concentration of released drug by measuring the UV-vis (ultraviolet visible) spectroscopy absorbance at 266 nm. The equal amount of the withdrawn volumes of the dialysates were returned to aqueous medium to reconstitute the original volume of PBS. The amount of drug released was plotted against time.

2.7. Cytotoxicity Assays

The cytotoxicity of the nanoparticles and drug nanoconjugates in the HEK293, MCF-7 and HeLa cell lines was investigated using MTT and SRB assays. Cells (2.0×10^4 per well) were seeded in 96-well plates containing 100 µL growth medium, and incubated at 37 °C in a 5% CO₂ incubator for 24 h. Thereafter, the medium was replaced with a fresh medium, and cells were treated with varying concentrations of the nanoparticles and nanoconjugates for 48 h.

2.7.1. MTT Assay

After 48 h, the spent medium was removed, and fresh growth medium containing 10% MTT solution was added to the cells and incubated for 4 h. Thereafter, the medium/MTT solution was removed and 100 µL DMSO was added to solubilize the formazan crystals. Control cells not treated with nanoparticles/nanocomposites were included as a positive control. All assays were done in triplicates. The absorbances were read at 540 nm in a Mindray MR- 96A microplate reader (Vacutec, Hamburg, Germany), and the percentage cell viability was estimated using the equation:

$$\% \text{ Cell viability} = \frac{\text{absorbance of treated cells}}{\text{absorbance of untreated cells}} \times 100$$

2.7.2. SRB Assay

After the incubation period, the cells were fixed with 25 µL cold tricarboxylic acid (TCA) (50%), and then incubated for 1 h at 4 °C. The cells were then gently washed (3×) with distilled water to remove residual TCA and serum proteins. The plate was then air-dried, and 50 µL of SRB (0.4% in 1% acetic acid) was added to the cells and incubated at 37 °C for 30 min, followed by washing (3×) with acetic acid (1%) and air drying. Finally, the dried cellular bound protein dye was solubilized in 100 µL of Tris buffer (10 mM, pH 10.5), and absorbances were measured as 3.28 at 565 nm, using the Tris base as the blank.

2.8. Apoptosis Assay

The acridine orange (AO)/ethidium bromide (EB) dual staining method [14] was used to investigate the effect of the pre-determined half maximal inhibitory concentrations (IC_{50}) of 5-FU encapsulated carriers on cell apoptosis. Briefly, cells (4.5×10^5 per well) were seeded in a 24-well plate and incubated for 24 h. Thereafter, the cells were exposed to the above samples for 24 h at 37 °C. Untreated cells were used as positive controls. Subsequently, cells were rinsed with cold PBS, and the dual stain (10 μ L) (AO: 0.1 mg.mL⁻¹, EB: 0.1 mg.mL⁻¹ in PBS) was added to the cells and allowed to stain for 5 min. Thereafter, the cells were briefly rinsed with cold PBS (200 μ L) and viewed under an Olympus fluorescent microscope (200 \times magnification), and images were captured with a CC12 fluorescent camera (Olympus Co., Tokyo, Japan). The apoptotic index was estimated using the following equation:

$$\text{Apoptotic index} = \text{number of apoptotic cells}/\text{number of total cells counted}$$

2.9. Statistics

Statistical analysis of the data was carried out using two-way ANOVA and Tukey's multiple comparison test (GraphPad Instat 6) across all groups. Differences were considered statistically significant at ** $p < 0.01$ and * $p < 0.05$.

3. Results and Discussion

3.1. Nanoparticle Characterization

Nanocomposite morphology was determined by transmission electron microscopy (TEM) analysis (Figure 1), which revealed spherical magnetic nanoparticles (MNPs) ($Mg_{0.5}Co_{0.5}Fe_2O_4$) with an average diameter of 11.6 nm and a narrow size distribution. No morphological changes were observed upon the functionalization and drug-loading of the CS- $Mg_{0.5}Co_{0.5}Fe_2O_4$ nanoparticles (NPs). However, there was a size increase of up to 20.4 nm, as recorded in Table 1.

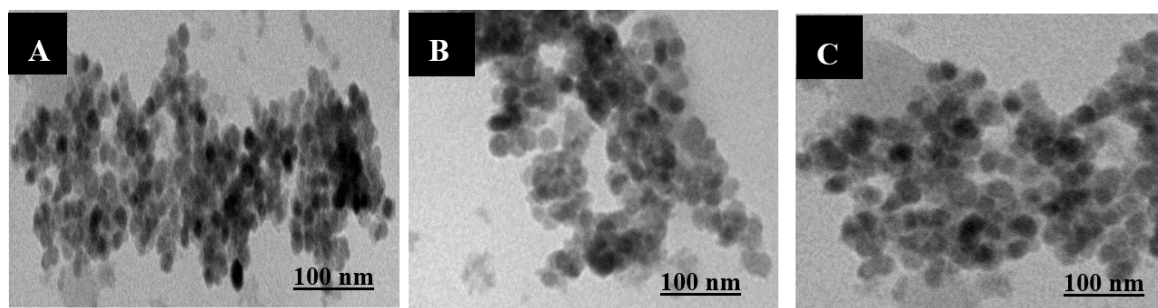


Figure 1. TEM images of (A) $Mg_{0.5}Co_{0.5}Fe_2O_4$, (B) CS- $Mg_{0.5}Co_{0.5}Fe_2O_4$ and (C) CS- $Mg_{0.5}Co_{0.5}Fe_2O_4$ -5FU NPs.

Table 1. TEM size diameter (TSD), hydrodynamic size diameter (HSD) and zeta potential (ζ) of the synthesized MNPs.

Samples	TSD	HSD (nm)	ζ (mV)
$Mg_{0.5}Co_{0.5}Fe_2O_4$	11.6 ± 0.3	64.9 ± 49.9	1.3 ± 1.2
CS- $Mg_{0.5}Co_{0.5}Fe_2O_4$	14.6 ± 0.7	129.4 ± 5.6	-9.7 ± 0.0
CS- $Mg_{0.5}Co_{0.5}Fe_2O_4$ -5-FU	20.4 ± 0.9	140.3 ± 8.9	-20.6 ± 0.2

Nanoparticle tracking analysis (NTA) measurements were carried out to determine sizes in colloidal suspensions. From the hydrodynamic sizes of MNPs (Table 1), it can be observed that the size diameter increased upon MNP functionalization with chitosan and the encapsulation of 5-fluorouracil (5-FU), from 64.9 ± 49.9 nm in $Mg_{0.5}Co_{0.5}Fe_2O_4$ NPs to 140.3 ± 8.9 nm in CS- $Mg_{0.5}Co_{0.5}Fe_2O_4$ -5FU

NPs. HSD ranges were expectedly more extensive compared to the dry TEM sizes. Similar reported results attributed the increase to the possible swelling of the chitosan-coated NPs in an aqueous environment [22]. Another reason is that with the nanocrystalline NPs being prone to agglomeration in solution, there is formation of nanoclusters [23].

The zeta potential magnitude is an indication of the repulsive forces or charges between particles in suspension, and can be used to foresee the stability of colloidal dispersions. The uncoated MNPs stabilized upon functionalization with chitosan, as evidenced by a zeta potential value from near-neutral and a positive 1.3 mV to -9.7 mV (Table 1). CS-Mg_{0.5}Co_{0.5}Fe₂O₄-5FU NPs displayed greater stability, as represented by zeta potential values of approximately -20.6 mV, in contrast to the non-drug bound CS-Mg_{0.5}Co_{0.5}Fe₂O₄ NPs. These were surprisingly unexpected, however, as chitosan is cationic in nature. While these values were in contradiction with most literature [24–27], reports of chitosan NPs displaying negative zeta potential have been noted [28].

Fourier Transform infra-red (FTIR) spectral analysis confirmed the presence of chitosan and 5-FU in CS-Mg_{0.5}Co_{0.5}Fe₂O₄-5FU nanocomposites (Figure 2). From the chitosan spectrum, the amide group was confirmed by its distinctive absorption peak at 1660 cm⁻¹. A characteristic IR band observed at 3484 cm⁻¹ was assigned to the O–H stretch, overlaid to the N–H stretching band and inner hydrogen bonds of the polysaccharide, indicating the remaining amino and hydroxyl groups providing the coordination ability with the metals. The characteristic absorption peak at 543 cm⁻¹ from the CS-Mg_{0.5}Co_{0.5}Fe₂O₄ spectrum is attributed to the Fe–O bond, which indicates formation of a cubic spinel structure. In the IR spectra of the drug, peaks in the 2800 – 2900 cm⁻¹ region were characteristic of the C–H stretching, while bands in 1431 – 1658 cm⁻¹ region were assigned to the C=C and C=N stretching vibrations. The bands around 1340 cm⁻¹ were vibrations of the pyrimidine compound. The absorption bands at 1178 and 1256 cm⁻¹ were C–O and C–N vibrations, respectively. The characteristic peaks of 5-FU were significantly weakened in the footprint region of the drug, strongly suggesting its encapsulation by chitosan functionalized MNPs.

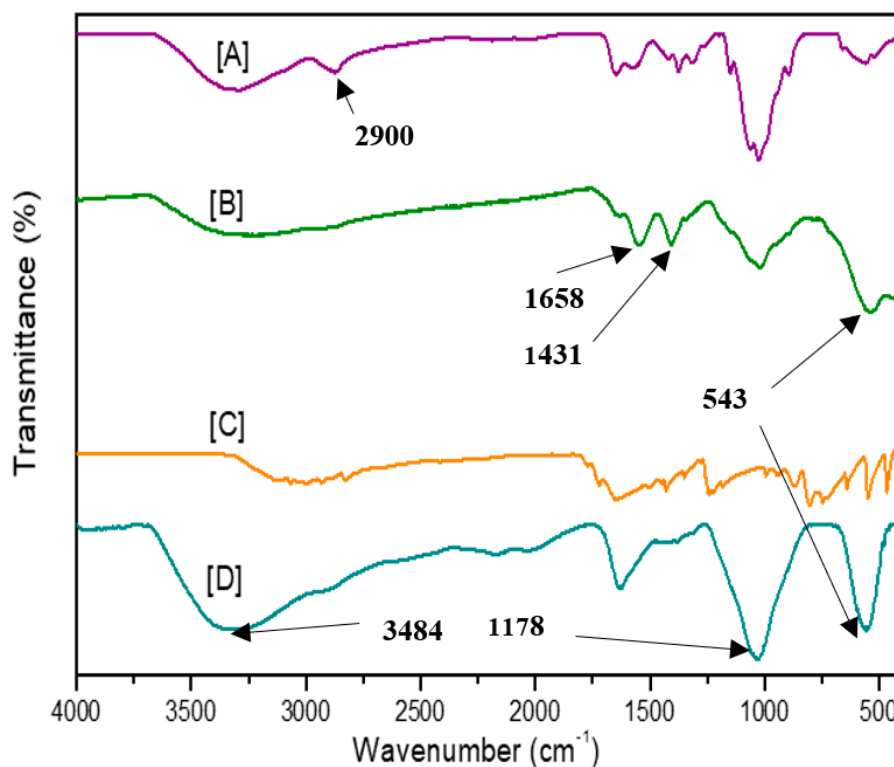


Figure 2. FTIR spectra of (A) Chitosan, (B) CS-Mg_{0.5}Co_{0.5}Fe₂O₄, (C) 5-FU and (D) CS-Mg_{0.5}Co_{0.5}Fe₂O₄-5FU NPs.

The typical bands of chitosan with minor shifts in CS-Mg_{0.5}Co_{0.5}Fe₂O₄-5FU-NPs confirmed the presence of chitosan on these formulated nanocarriers. However, some of the other bands around 1200–900 cm⁻¹ in chitosan (Figure 2A) were observed to have diminished following drug encapsulation. This could be due to potential degradation of low molecular weight chitosan [29]. Additionally, the peaks around 1658 and 1178 cm⁻¹ were observed to have intensified with the loading of 5-FU (Figure 2D). The assignment of peaks correlated to those in literature [30,31].

3.2. Encapsulation Efficiency (EE)

The EE of 5-FU within CS-Mg_{0.5}Co_{0.5}Fe₂O₄ NPs was determined using UV-vis (ultraviolet visible) spectroscopy. The EE of 5-FU was estimated based on the amount of 5-FU present in the supernatant during dialysis. CS-Mg_{0.5}Co_{0.5}Fe₂O₄-5FU NPs demonstrated an EE of 67%, which also explains TEM and NTA results showing that CS-Mg_{0.5}Co_{0.5}Fe₂O₄ was large in size, and provided a large surface area to bind 5-FU. The EE results by Tummala et al. were also found to be in the range of 60% [19].

3.3. Release Studies

The drug release from the nanoparticles can occur in two ways: sudden release and sustained release. The sudden release of the drug is caused by the drug adsorbed onto the surface of the nanoparticles, while the sustained release is caused by the degradation of the carrier matrix and the slow diffusion of the drug from the polymer matrix [19]. The in vitro drug release patterns of 5-FU from the CS-Mg_{0.5}Co_{0.5}Fe₂O₄-5FU NPs at pH 4.5, 6.5 and 7.4 are shown in Figure 3. These conditions were chosen to mimic the acidic tumor environment and physiological environment, such as blood with a near neutral pH. Approximately, 97%, 73% and 73% of the drug was cumulatively released from CS-Mg_{0.5}Co_{0.5}Fe₂O₄-5FU NPs at pH 4.5, 6.5 and 7.4, respectively, after 48 h.

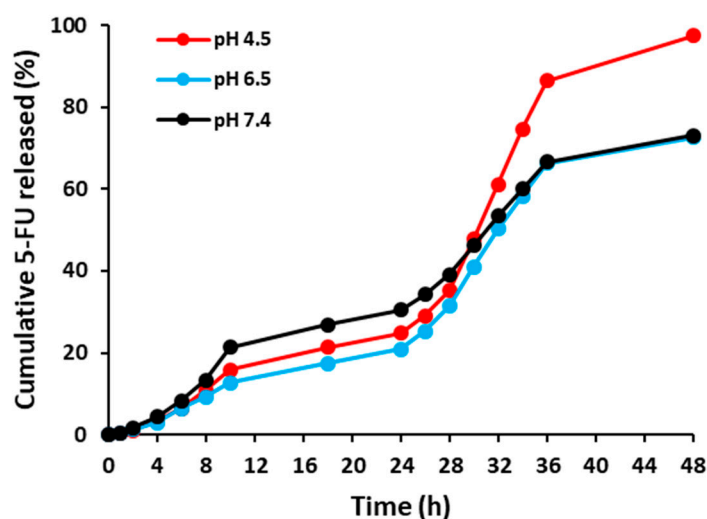


Figure 3. In vitro drug release profiles of 5-FU from CS-Mg_{0.5}Co_{0.5}Fe₂O₄-5FU NPs.

In the acidic buffer solution, the drug release rate was relatively rapid in comparison to that of a neutral buffer solution. The observation can be attributed to the residual amine (–NH₂) groups that are protonated at this pH, leading to a repulsive force between the adjacent positive charges. As this happens, it would cause the polymer to swell up, leading to more of the drug diffusing out [24]. At pH 7.4, however, the amine groups tend to attach closely to the surface of the NP, which means there is a slowed-down release of the drug. These findings were consistent with reports in literature [32–34]. Another reason may relate to the increased solubility of chitosan at acidic pH [32]. A sustained and pH-dependent release is preferred, as it means that the drug can be administered over time for better efficacy, especially in targeted anti-cancer delivery.

3.4. Cytotoxicity (MTT and SRB) Assays

3-[(4,5-dimethylthiazol-2-yl)-2,5-diphenyl tetrazolium bromide] (MTT) and sulforodhamine B (SRB) assays were carried out to evaluate the cytotoxic effect of the drug-free carriers, and free 5-FU and its encapsulated nanocomposites on human breast adenocarcinoma (MCF-7), human cervical cancer (HeLa) and human embryonic kidney (HEK293) cells after 48 h. The MTT assay is based on the principle that only viable cells with a functional mitochondrial dehydrogenase enzyme can reduce MTT to an insoluble formazan product. The SRB assay is based on the principle that under mild acidic conditions, the anionic protein dye SRB electrostatically binds to basic amino acid residues of tricarboxylic acid (TCA)-fixed cells. These two assays differ in sensitivity, and a comparison of the results attained in both assays will provide a good initial assessment of the safety of the 5-FU-loaded nanocomposites. The cytotoxicity induced and half maximal inhibitory (IC_{50}) values of the investigated nanocarriers are represented in Figures 4 and 5 and Tables 2 and 3, respectively. The drug-free MNPs were nontoxic to all cell lines in both assays. Hence, it can be inferred that any cytotoxicity observed in the cancer cells was due to the drug rather than the nanocarriers.

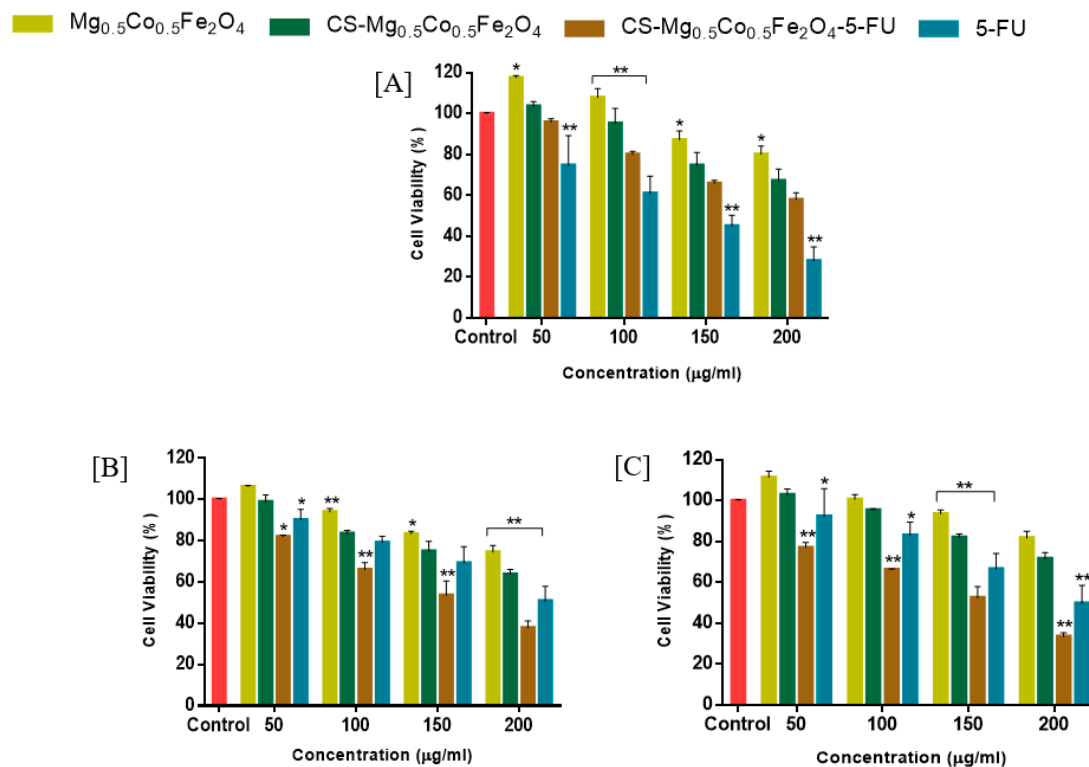


Figure 4. MTT cell viability assay in human cell lines (A) HEK293, (B) MCF-7, and (C) HeLa. (** $p < 0.01$, * $p < 0.05$) was considered statistically significant, and the mean data is represented as means \pm SD ($n = 3$).

Table 2. IC_{50} values of free 5-FU and 5-FU-loaded nanocomposites in HEK293, MCF-7 and HeLa cells for the MTT assay.

Samples	IC_{50} Calculation ($\mu\text{g/mL}$)		
	HEK293	MCF-7	HeLa
$CS-Mg_{0.5}Co_{0.5}Fe_2O_4-5FU$	251	158	158
5-FU	126	251	251

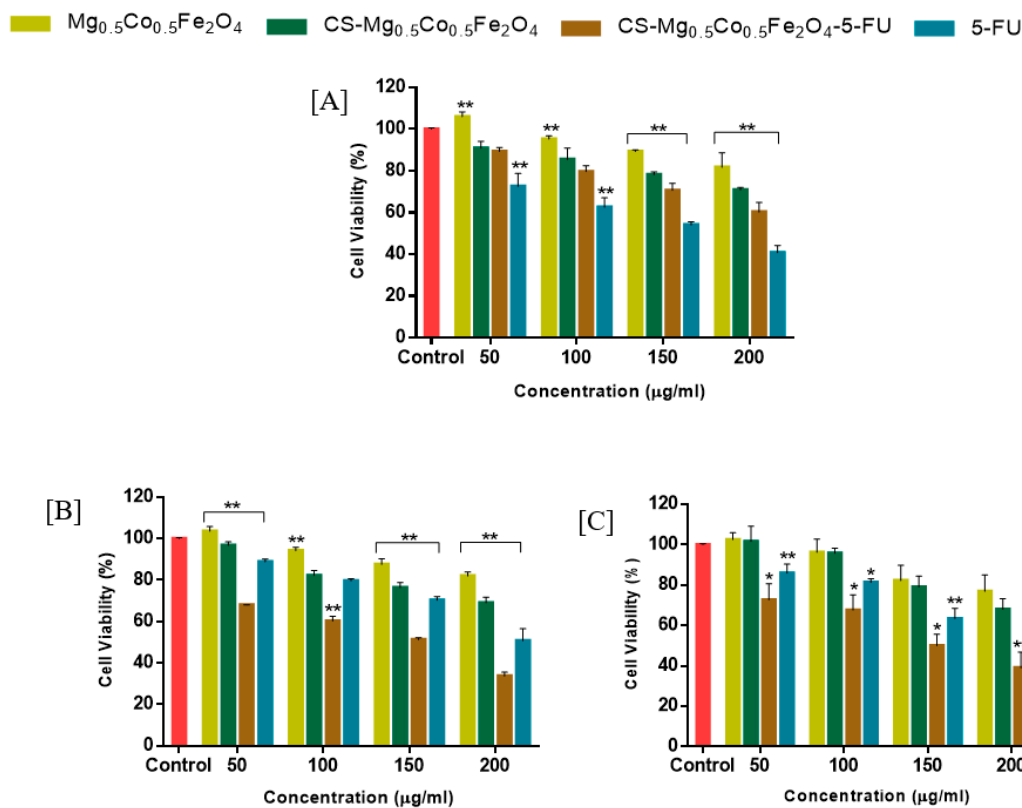


Figure 5. SRB cell viability assay in human cell lines (A) HEK293, (B) MCF-7, and (C) HeLa. (** $p < 0.01$, * $p < 0.05$) was considered statistically significant and the mean data is represented as means \pm SD ($n = 3$).

Table 3. IC₅₀ values of free 5-FU and 5-FU-loaded nanocomposites in HEK293, MCF-7 and HeLa cells for the SRB assay.

Samples	IC ₅₀ Calculation (µg/mL)		
	HEK293	MCF-7	HeLa
CS-Mg _{0.5} Co _{0.5} Fe ₂ O ₄ -5-FU	398	158	126
5-FU	158	251	251

Cytotoxicity studies of the nanocomposites were carried out using non-cancerous HEK293 as control cell lines, as illustrated in Figures 4A and 5A. CS-Mg_{0.5}Co_{0.5}Fe₂O₄-5FU NPs were found to be nontoxic to the HEK293 cells, even at the highest studied concentration of 200 µg/mL, with >55% cell viability in both the MTT and SRB assays. In contrast, the free drug (5-FU) elicited >60% cell death in the HEK293 cells at 200 µg/mL in both assays. This indicated that these drug nanocomposites were well tolerated in the non-cancerous cells. Hence, these chitosan functionalized nanocarriers show the potential to be safe nanocarriers, even at higher dosages.

CS-Mg_{0.5}Co_{0.5}Fe₂O₄-5FU NPs were seen to be toxic in the MCF-7 cells at 200 µg/mL, causing approximately 60% (Figures 4B and 5B) cell death in both assays, while the free drug at similar concentrations had <50% cell death. IC₅₀ values of 158 and 398 µg/mL (Tables 2 and 3) for CS-Mg_{0.5}Co_{0.5}Fe₂O₄-5FU NPs were recorded for the MTT and SRB assays, respectively.

Furthermore, CS-Mg_{0.5}Co_{0.5}Fe₂O₄-5FU NPs exhibited over 65% cell death in the HeLa cells (Figures 4C and 5C) for both assays at 200 µg/mL, while 5-FU exhibited 50% cell death at a similar concentration. CS-Mg_{0.5}Co_{0.5}Fe₂O₄-5FU NPs had IC₅₀ values of 158 and 126 µg/mL in the HeLa cells for the MTT and SRB assays, respectively. The enhanced cytotoxicity exhibited by CS-Mg_{0.5}Co_{0.5}Fe₂O₄-5FU NPs in the MCF-7 and HeLa cells, compared to the free drug, may be attributed to the ability of

the functionalized $\text{Mg}_{0.5}\text{Co}_{0.5}\text{Fe}_2\text{O}_4$ -5FU NPs to evade cellular barriers, and promoting the controlled release and accumulation of 5-FU in the tumor cells. The results obtained correlate with the drug release studies, where CS- $\text{Mg}_{0.5}\text{Co}_{0.5}\text{Fe}_2\text{O}_4$ -5FU displayed a prolonged and steady drug release, hence enhancing the therapeutic effect of 5-FU by delivering it gradually to the acidic tumor environment. Therefore, it is apparent that these drug-encapsulated nanocomposites exhibit anti-proliferative activity, especially in the cancer cells, while they are nontoxic in the non-cancer cells. The obtained results were in agreement with previous reports, where the cytotoxic effect of chitosan functionalized MNPs not bound to anticancer drugs were relatively nontoxic to cells.

3.5. Apoptosis Assay

The acridine orange (AO)/ethidium bromide (EB) dual staining assay was used to detect any morphological changes induced when the cytotoxic agents were administered at IC_{50} concentrations (Tables 2 and 3). This assay was used as a correlation for any observed cytotoxicity in the MTT and SRB assays for free 5-FU and the CS- $\text{Mg}_{0.5}\text{Co}_{0.5}\text{Fe}_2\text{O}_4$ -5FU NPs. This staining technique is based on the principle that viable cells have double-stranded DNA, and display green fluorescence upon staining with AO, while non-viable cells are characterized by single-stranded DNA and fluoresce yellow to red when stained with EB [21]. Apoptotic indices and microscopic cell images are shown in Table 4 and Figure 6 respectively.

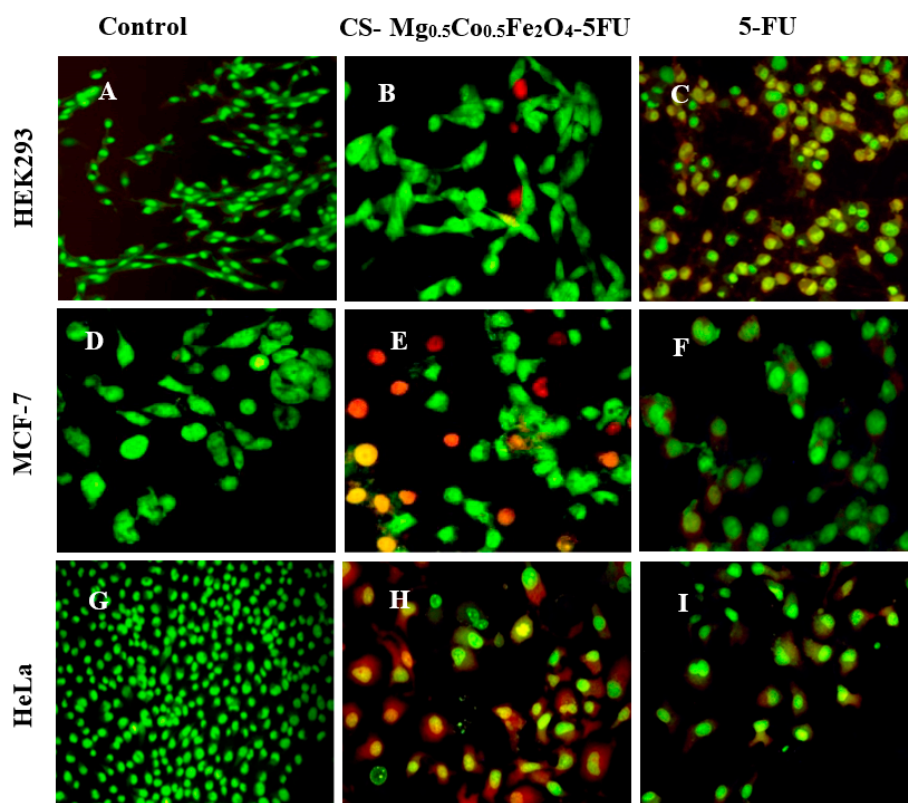


Figure 6. Fluorescent images of AO/EB stained cells (A) HEK293 control cells, (B) HEK293 cells treated with CS- $\text{Mg}_{0.5}\text{Co}_{0.5}\text{Fe}_2\text{O}_4$ -5FU NPs, (C) HEK293 cells treated with 5-FU (D) MCF-7 control cells, (E) MCF-7 cells treated with CS- $\text{Mg}_{0.5}\text{Co}_{0.5}\text{Fe}_2\text{O}_4$ -5FU NPs, (F) MCF-7 cells treated with 5-FU, (G) HeLa control cells, (H) HeLa cells treated with CS- $\text{Mg}_{0.5}\text{Co}_{0.5}\text{Fe}_2\text{O}_4$ -5FU NPs and (I) HeLa cells treated with 5-FU. Images taken at 20 \times magnification.

Table 4. Apoptotic indices of free 5-FU and 5-FU-loaded nanocomposites.

Samples	Apoptotic Indices		
	HEK293	MCF-7	HeLa
CS-Mg _{0.5} Co _{0.5} Fe ₂ O ₄ -5FU	0.08	0.41	0.85
5-FU	0.28	0.25	0.33

All control cells fluoresced green after staining, indicating their viable states (Figure 6A,D,G). The lower apoptotic indices depicted in Table 4, and a high number of HEK293 cells which fluoresced green after staining (Figure 6B), demonstrated the relative nontoxic effects of the drug- nanocomposites. Interestingly, both MCF-7 and HeLa cells treated with CS-Mg_{0.5}Co_{0.5}Fe₂O₄-5FU NPs showed high apoptotic indexes of 0.41 and 0.85, respectively, when compared to cells treated with free 5-FU, suggesting the facilitated internalization of CS-Mg_{0.5}Co_{0.5}Fe₂O₄-5FU NPs by these cancer cells. Overall, these results are consistent with the cytotoxicity findings of the MTT and SRB assays, and further confirm the cancer cell-specific delivery of the CS-Mg_{0.5}Co_{0.5}Fe₂O₄-5FU NPs.

4. Conclusions

In this study, 5-fluorouracil (5-FU) was effectively encapsulated by the CS-Mg_{0.5}Co_{0.5}Fe₂O₄ nanoparticles (NPs), with chitosan serving as a functionalizing and stabilizing agent. Furthermore, the small sized and spherically shaped 5-FU nanocomposites showed high colloidal stability and sustained a pH-dependent drug release over 48 h, under acidic and physiological pH conditions. Enhanced and selective anticancer activities were observed for the CS-Mg_{0.5}Co_{0.5}Fe₂O₄-5FU NPs in both investigated cancer cells compared to the free drug, which is significant for the reduction of the dosage regimen and the prevention of off-target effects. From these results, it can be inferred that the synthesized chitosan functionalized magnetic nanoparticles are promising nanocarriers, and have the potential to be used as a pH-responsive drug delivery system, which can be targeted to cancer cells under a magnetic field. Further studies can be undertaken to explore the mechanisms of cellular uptake among NPs.

Author Contributions: Conceptualization, supervision, project administration, resources, and funding acquisition, S.M. (Seipati Mokhosi) and M.S.; methodology and investigation, software, formal analysis, and data curation, S.M. (Sanele Mngadi) and W.M.; writing—original draft preparation, S.M. (Sanele Mngadi) and M.S.; and writing—review and editing, funding S.M. (Seipati Mokhosi), M.S. and W.M. All authors have read and agreed to the published version of the manuscript.

Funding: This research was partially funded by the National Research Foundation of South Africa S.M. (Seipati Mokhosi) grant No.: 107407; M.S. grant No.: 113850; W.M. grant No.: 113860).

Conflicts of Interest: The authors declare no conflict of interest.

References

- Huang, J.; Li, Y.; Orza, A.; Lu, Q.; Guo, P.; Wang, L.; Yang, L.; Mao, H. Magnetic nanoparticle facilitated drug delivery for cancer therapy with targeted and image-guided approaches. *Adv. Funct. Mater.* **2016**, *26*, 3818–3836. [[CrossRef](#)] [[PubMed](#)]
- Unsoy, G.; Khodadust, R.; Yalcin, S.; Mutlu, P.; Gunduz, U. Synthesis of Doxorubicin loaded magnetic chitosan nanoparticles for pH responsive targeted drug delivery. *Eur. J. Pharm. Sci.* **2014**, *62*, 243–250. [[CrossRef](#)] [[PubMed](#)]
- Kudr, J.; Haddad, Y.; Richtera, L.; Heger, Z.; Cernak, M.; Adam, V.; Zitka, O. Magnetic nanoparticles: From design and synthesis to real world applications. *Nanomaterials* **2017**, *7*, 243. [[CrossRef](#)] [[PubMed](#)]
- Jauhar, S.; Kaur, J.; Goyal, A.; Singhal, S. Tuning the properties of cobalt ferrite: A road towards diverse applications. *RSC Adv.* **2016**, *6*, 97694. [[CrossRef](#)]
- Dey, C.; Baishya, K.; Ghosh, A.; Goswami, M.M.; Ghosh, A.; Mandal, K. Improvement of drug delivery by hyperthermia treatment using magnetic cubic cobalt ferrite nanoparticles. *J. Magn. Magn. Mater.* **2017**, *427*, 168–174. [[CrossRef](#)]

6. Pon-Ona, W.; Charoenphandhub, N.; Tang, I.; Jongwattanapisan, P.; Krishnamra, N.; Hoonsawat, R. Encapsulation of magnetic CoFe_2O_4 in SiO_2 nanocomposites using hydroxyapatite templates: A drug delivery system. *Mater. Chem. Phys.* **2011**, *131*, 485–494. [[CrossRef](#)]
7. Hathout, A.S.; Aljawish, A.; Sabry, B.A.; El-Nekeety, A.A.; Roby, M.H.; Deraz, N.M.; Aly, S.E.; Abdel-Wahhab, M.A.; Paul Langevin, B.; Cedex, A. Synthesis and characterization of cobalt ferrites nanoparticles with cytotoxic and antimicrobial properties. *J. Appl. Pharm. Sci.* **2017**, *7*, 86–92. [[CrossRef](#)]
8. Chomoucka, J.; Drbohlavova, J.; Huska, D.; Adam, V.; Kizek, R.; Hubalek, J. Magnetic nanoparticles and targeted drug delivering. *Pharmacol. Res.* **2010**, *62*, 144–149. [[CrossRef](#)]
9. Feng, O.; Liu, Y.; Huang, J.; Chen, K.; Huang, J.; Xiao, K. Uptake, distribution, clearance, and toxicity of iron oxide nanoparticles with different sizes and coatings. *Sci. Rep.* **2018**, *8*, 2082. [[CrossRef](#)]
10. Mushtaq, M.W.; Kanwal, F.; Batool, A.; Jamil, T.; Zia-ul-Haq, M.; Ijaz, B.; Huang, Q.; Ullah, Z. Polymer-coated CoFe_2O_4 nanoassemblies as biocompatible magnetic nanocarriers for anticancer drug delivery. *J. Mater. Sci.* **2017**, *52*, 9282–9293. [[CrossRef](#)]
11. Pineda, M.G.; Torres, S.; López, L.V.; Enríquez-Medrano, F.J.; de León, R.D.; Fernández, S.; Saade, H.; López, R.G. Chitosan-coated magnetic nanoparticles prepared in one-step by precipitation in a high-aqueous phase content reverse microemulsion. *Molecules* **2014**, *19*, 9273–9287. [[CrossRef](#)] [[PubMed](#)]
12. Manivasagana, P.; Nguyen, V.T.; Jun, S.W.; Hoanga, G.; Mondala, S.; Kim, H.; Doan, V.H.M.; Kim, J.; Kim, C.; Oh, J. Anti-EGFR antibody conjugated thiol chitosan-layered gold nanoshells for dual-modal imaging-guided cancer combination therapy. *J. Control. Release* **2019**, *311–312*, 26–42. [[CrossRef](#)] [[PubMed](#)]
13. Ali, A.; Ahmed, S. A review on chitosan and its nanocomposites in drug delivery. *Int. J. Biol. Macromol.* **2018**, *109*, 273–286. [[CrossRef](#)] [[PubMed](#)]
14. Moreno, J.A.S.; Mendes, A.C.; Stephansen, K.; Engwer, C.; Goycoolea, F.M.; Boisen, A.; Nielsen, L.H.; Chronakis, I.S. Development of electrosprayed mucoadhesive chitosan microparticles. *Carbohydr. Polym.* **2018**, *190*, 240–247. [[CrossRef](#)]
15. Lu, K.; Lin, Y.; Lu, H.; Ho, Y.; Weng, S.; Tsai, M.; Mi, F. A novel injectable *in situ* forming gel based on carboxymethyl hexanoyl chitosan/hyaluronic acid polymer blending for sustained release of berberine. *Carbohydr. Polym.* **2018**, *206*, 664–673. [[CrossRef](#)]
16. Wang, Y.; Xie, M.; Ma, G.; Fang, Y.; Yang, W.; Ma, N.; Fang, D.; Hu, Q.; Pei, F. The antioxidant and antimicrobial activities of different phenolic acids grafted onto chitosan. *Carbohydr. Polym.* **2019**, *225*, 115238. [[CrossRef](#)]
17. Li-Chu Tsai, L.; Chen, C.; Lin, C.; Ho, Y.; Mi, F. Development of multifunctional nanoparticles self-assembled from trimethyl chitosan and fucoidan for enhanced oral delivery of insulin. *Int. J. Biol. Macromol.* **2019**, *126*, 141–150. [[CrossRef](#)]
18. Mu, Y.; Fu, Y.; Lia, J.; Yu, X.; Lia, Y.; Wang, Y.; Wu, X.; Zhang, K.; Kong, M.; Feng, C.; et al. Multifunctional quercetin conjugated chitosan nano-micelles with P-gp inhibition and permeation enhancement of anticancer drug. *Carbohydr. Polym.* **2019**, *203*, 10–18. [[CrossRef](#)]
19. Sun, L.; Chen, Y.; Zhou, Y.; Guo, F.; Zheng, Y.; Chen, W. Preparation of 5-fluorouracil-loaded chitosan nanoparticles and study of the sustained release *in vitro* and *in vivo*. *Asian J. Pharm. Sci.* **2017**, *12*, 418–423. [[CrossRef](#)]
20. Tummala, S.; Satish Kumar, M.N.; Prakash, A. Formulation and characterization of 5-Fluorouracil enteric coated nanoparticles for sustained and localized release in treating colorectal cancer. *Saudi Pharm. J.* **2015**, *23*, 308–314. [[CrossRef](#)]
21. Dlamini, W.B.; Msomi, J.Z.; Moyo, T. XRD, Mössbauer and magnetic properties of $\text{Mg}_x\text{Co}_{1-x}\text{Fe}_2\text{O}_4$ nanoferrites. *J. Magn. Magn. Mater.* **2015**, *373*, 78–82. [[CrossRef](#)]
22. Khalkhali, M.; Rostamizadeh, K.; Sadighian, S.; Khoeini, F.; Naghibi, M.; Hamidi, M. The impact of polymer coatings on magnetite nanoparticles performance as MRI contrast agents: A comparative study. *Daruj. Pharm. Sci.* **2015**, *23*, 45. [[CrossRef](#)]
23. Singh, M.; Akinyelu, J. Folic acid-conjugated chitosan functionalised gold nanoparticles for targeted delivery of 5-Fluorouracil in breast cancer. In Proceedings of the 3rd World Congress on Recent Advances in Nanotechnology, Budapest, Hungary, 10–12 April 2018; p. 103. [[CrossRef](#)]
24. Prabha, G.; Raj, V. Preparation and characterization of polymer nanocomposites coated magnetic nanoparticles for drug delivery applications. *J. Magn. Magn. Mater.* **2016**, *408*, 26–34. [[CrossRef](#)]
25. Arum, Y.; Oh, Y.; Kang, H.; Ahn, S.; Oh, J. Chitosan-coated Fe_3O_4 magnetic nanoparticles as carrier of cisplatin for drug delivery. *Fish. Aquat. Sci.* **2015**, *18*, 89–98. [[CrossRef](#)]

26. Zamora-Mora, V.; Fernández-Gutiérrez, M.; Román, J.S.; Goya, G.; Hernández, R.; Mijangos, C. Magnetic core-shell chitosan nanoparticles: Rheological characterization and hyperthermia application. *Carbohydr. Polym.* **2014**, *102*, 691–698. [[CrossRef](#)]
27. Zamora-Mora, V.; Fernández-Gutiérrez, M.; González-Gómez, Á.; Sanz, B.; Román, J.S.; Goya, G.F.; Hernández, R.; Mijangos, C. Chitosan nanoparticles for combined drug delivery and magnetic hyperthermia: From preparation to *in vitro* studies. *Carbohydr. Polym.* **2017**, *157*, 361–370. [[CrossRef](#)]
28. Soares, S.F.; Fernandes, T.; Sacramento, M.; Trindade, T.; Daniel-da-Silva, A.L. Magnetic quaternary chitosan hybrid nanoparticles for the efficient uptake of diclofenac from water. *Carbohydr. Polym.* **2018**, *203*, 35–44. [[CrossRef](#)]
29. Islam, N.; Dmour, I.; Taha, M.O. Degradability of chitosan micro/nanoparticles for pulmonary drug delivery. *Heliyon* **2019**, *5*, e01684. [[CrossRef](#)]
30. Mund, H.S.; Ahuja, B.L. Structural and magnetic properties of Mg doped cobalt ferrite nano particles prepared by sol-gel method. *Mater. Res. Bull.* **2017**, *85*, 228–233. [[CrossRef](#)]
31. Zeinali, S.; Nasirimoghaddam, S.; Sabbaghi, S. Investigation of the synthesis of chitosan coated iron oxide nanoparticles under different experimental conditions. *Int. J. Nanosci. Nanotechnol.* **2016**, *12*, 183–190.
32. Mohammed, M.A.; Syeda, J.T.M.; Wasan, K.M.; Wasan, E.K. An overview of chitosan nanoparticles and its application in non-parenteral drug delivery. *Pharmaceutics* **2017**, *9*, 53. [[CrossRef](#)]
33. Ding, Y.; Shen, S.Z.; Sun, H.; Sun, K.; Liu, F.; Qi, Y.; Yan, J. Design and construction of polymerized-chitosan coated Fe₃O₄ magnetic nanoparticles and its application for hydrophobic drug delivery. *Mater. Sci. Eng. C* **2015**, *48*, 487–498. [[CrossRef](#)]
34. Maney, V.; Singh, M. An *in vitro* assessment of novel chitosan/bimetallic PtAu nanocomposites as delivery vehicles for doxorubicin. *Nanomedicine* **2017**, *12*, 2625–2640. [[CrossRef](#)]



© 2020 by the authors. Licensee MDPI, Basel, Switzerland. This article is an open access article distributed under the terms and conditions of the Creative Commons Attribution (CC BY) license (<http://creativecommons.org/licenses/by/4.0/>).